Simultaneous pore enlargement and introduction of highly dispersed Fe/Cu active sites in MSNs/SBA-15, respectively, for enhanced catalytic activity

S. P. ELANGOVAN*
and Jinlou GU

An effective post hydrothermal treatment strategy has been developed to dope highly dispersed catalytically active iron centers into the framework of Mesoporous silica Nanoparticles (MSNs) and copper centers into the framework of rod-like SBA-15, with simultaneous expansion of pore size of the synthesized MSNs or SBA-15; here, MSNs and SBA-15 are collectively denoted as Mesoporous silica, for convenience. The hydrophobic core of the surfactant micelle in the as-synthesized Mesoporous silica was effectively employed as a carrier for the hydrophobic precursors of corresponding metal acetyl acetonate ($Fe(acac)_3$ or $Cu(acac)_2$) during hydrothermal treatment (HT) before surfactant removal; and the metal derived catalysis centers within Mesoporous silica were strategically generated on pyrolysis. Characterization techniques such as XRD, BET, SEM and TEM support that the synthesized Fe-MSNs are long period ordered with particles size about 100 nm and a relatively large pore size of *ca*. 3.5 nm. UV-Vis, measurements demonstrate that the introduced iron active centers are highly dispersed in a coordinative unsaturated status. NH_3-TPD verifies that the acid amount of iron-doped MSNs is quite high. The synthesized nanocatalysts show an excellent catalytic performance for benzylation of benzene by benzyl chloride, and they present relatively higher yield and selectivity to diphenylmethane with lower iron content and much shorter reaction time. In the case of Cu doped on SBA-15, characterizations of the synthesized samples by a series of techniques such as XRD, TEM, BET, TPR, UV–Vis, and ICP–AES manifested that about 0.19-0.85 wt. % copper was directly introduced and dispersed into the inner surface of SBA-15 pore network. While there were few studies, if any, to utilize synthetic copper catalysts for the selective oxidation of cyclohexane oxidation, it was found that currently synthesized Cu-SBA-15 demonstrated very interesting catalytic properties for this industrially important reaction. Under the optimized reaction condition at an oxygen pressure of 1MPa and a temperature of 120 °C for 7 h, the conversion of cyclohexane to the target products was higher than 11 %, meanwhile, the total selectivity to cyclohexanol and cyclohexanone satisfactorily reached to *ca*. 80 %.

Keywords: Nanotechnology; Mesoporous silica; Self-assembly; Pore expansion; Catalyst; Cyclohexane oxidation; Alkylation;

1 Introduction

Ordered mesoporous silica (OMS), which were first synthesized by scientists from Mobil[1,2], possess high surface area and tunable porous structure. They have attracted tremendous interest in the past decade owing to their broad applications, especially in heterogeneous catalytic processes involving large molecules[3,4]. However, for pure silica, there are few catalytically active sites on its amorphous SiO_2 framework in contrast to the fact that zeolites usually possess a large number of isolated active sites. Consequently, many successful synthetic methods have been developed to prepare mesoporous silica with isomorphous substitution of hetero-elements such as aluminum, gallium, titanium, vanadium, manganese and iron into silica framework for obtaining high-performance catalysts or catalyst supports. Another issue needs to be solved is how to guarantee the full accessibility of the catalytically active centers. To make the introduced active centers work efficiently, a general strategy is to reduce the particle size of bulky OMS as far as possible, e.g. down to the nanometer scale and many efforts have been recently made to prepare this type of nanocatalyst support. On the other hand, the pore diameter of the reported mesoporous silica nanoparticles (MSNs) which is generally templated by cetyltrimethylammonium bromide (CTAB), is as small as about 2.5 nm5). Such a relatively small pore size will also prevent the reagents with larger sizes from accessing the catalytically active centers. To some extent, this will counteract the advantages benefiting from the reduction of particle size. Therefore, it is still highly desirable to prepare the nanosized mesoporous catalysts with uniformly dispersed heterogeneous atoms as catalytically active centers at the inner pore surface, and simultaneously, with enlarged pore diameters.

Currently, there are several available methods to expand the pore size of OMS6), while the most commonly used technique is the introduction of a swelling agent such as trimethylbenzene (TMB) into the structure directing template, either in the preparation step7) or in the post hydrothermal treatment (HT)8). It was proposed that TMB molecules tend to locate themselves in the hydrophobic interiors of the surfactant micelles, leading to the increased micelle diameter, and consequently the enlarged pore size of the resulting OMS. Actually, the hydrophobic region of surfactant micelle could provide the compatible environment for accommodating the hydrophobic compounds, not only for swelling agents such as pure chemical solvent of TMB, but also for some metal complexes such as hydrophobic ferric acetylacetonate (Fe(acac)$_3$), which would enhance the overall solubility of hydrophobic compounds in the hydrophobic core and prevent their aggregation9). After the in situ pyrolysis of the metallic precursors, the resultant metallic species can be highly dispersed within the mesopore channels since the surfactant is only encapsulated in the pore channels of OMS during the self-assembly10). These imply that the introduction of metallic heteroatoms into silica framework and pore expansion of OMS can be simultaneously achieved if the mixture solution of TMB and hydrophobic metallic precursors was used to serve as a swelling agent.

Generally, the reported methods for small size MSN preparation were direct sol-gel process in a heated solvent such as in water at 80 °C or water-ethanol mixtures at 40-50 °C without HT. The average pore size of the MSN was around 2.5 nm when the cationic surfactant of CTAB was used as the structure directing agent. To expand the pore size, a swelling agent could be introduced either in the preparation step or in the post HT. However, the process for MSN preparation is very sensitive to the synthesis conditions. Especially, when large amount of additives such as Fe(acac)$_3$ or TMB are added to the parent solution, it will destroy the ordering structure of the obtained MSNs. Additionally, since MSNs are generally prepared in strong alkaline media such as NaOH or NH$_4$OH aqueous solution, high concentration OH$^-$ of will inevitably attack the hydrophobic compounds such as Fe(acac)$_3$ and changes its inherent hydrophobicity to hydrophilicity, which will make the metallic compounds undissolvable in the hydrophobic cores of the surfactant11). Therefore, post HT seems more suitable for the pore expansion of the synthesized MSNs using the mixture solution of TMB with Fe(acac)$_3$ dissolved. During the sol-gel process for parent MSN preparation, the morphology and the particle size have been completely controlled by a simple surfactant templated, base-catalyzed condensation procedure. Then during the subsequent HT procedure without removing the surfactant from MSNs, TMB and Fe(acac)$_3$ will be co-infiltrated into the hydrophobic core of CTAB micelles as both the pore expander and iron precursor. Large pore size will be produced in the final obtained MSNs due to the expanding effect of the hydrophobic compounds and highly dispersed iron active centers will be also created upon subsequent pyrolysis.

Supported copper catalysts have also attracted considerable attentions due to their recent practical uses in many heterogeneous redox reactions12). Mesoporous materials (MMs), such as SBA-15 with intrinsically high surface area and pore volume13), could serve as an excellent platform for their deposition14). To enhance the catalytic efficiency of the incorporated copper species and take full advantages of the supports, uniform dispersion of the active centers is preferable for free access by the reactants15). Simultaneously, the size of copper species in the form of nanoparticles, clusters or isolated copper ions should be controlled at least below the pore size of employed mesoporous supports to prevent the pore blocking and also ensure enough active surface exposure to the reactants.

Generally, two preparative routes i.e. the post modification16) and one-pot synthesis17) have been followed for the introduction of active copper catalytic centers. Using post modification methods, such as wet impregnation or deposition-precipitation, the procedure is relatively controllable since the parent support preparation and the grafting process are totally separated, however it is quite difficult to obtain the uniformly distributed copper species within MMs. Comparatively, the one-pot direct method produces better control over the distribution of the introduced copper species since all the reagents for the catalyst preparation are uniformly mixed together but generally at the expense of the mesoscopic ordering of the support. Keeping the pros and cons of the two existent routes in mind, herein, a novel and controllable strategy is developed to introduce highly dispersed copper species into rod-like mesoporous SBA-15 silica.

It is currently well known that the hydrophobic core of P123 micelles for SBA-15 templating could provide the compatible environment for the hydrophobic compound, such as Cu(acac)$_2$ in our current case[18]. However, the SBA-15 is usually synthesized in strong acid media, e.g. 2M HCl[19]; such harsh environment will make copper precursor unstable if we employ a one-pot synthesis strategy. Therefore, similar to that of Fe/MSNs, parent SBA-15 was prepared at first without introducing copper-containing hydrophobic compounds and separated the SBA-15/P123 from its mother solution. Then during the subsequent hydrothermal procedure, hydrophobic compound of Cu(acac)$_2$ was added as the copper source and spontaneously infiltrated into the hydrophobic core of P123 micelles. Followed by pyrolysis, the catalytic centers of copper within SBA-15 were strategically prepared. The synthesized catalysts demonstrated excellent catalytic properties for the selective oxidation of cyclohexane[20]. In comparison with a 4 % conversion using traditionally commercial cobalt-based catalysts, the conversion of cyclohexane to the target products was higher than 11 % over the synthesized highly dispersed copper catalysts within SBA-15 under a relatively mild experimental condition.

So, the present work reports a novel and controllable post HT method and intend to solve three issues together, i.e. to dope the highly dispersed iron catalytically active centers into the framework of MSNs, to keep the particle size in nanometric scale and simultaneously to expand the pore size of the synthesized MSNs. We also demonstrate that the synthesized nanocatalysts show excellent catalytic performance for benzylation of benzene by benzyl chloride (BC), a very important Friedel–Crafts alkylation reactions commonly used in organic chemistry[21]. In addition, this newly developed method was adopted to fabricate Cu-SBA-15 catalysts and reveals the highly dispersed nature of the incorporated copper species at the inner surface of Mesoporous silica framework. The significantly enhanced catalytic activity for cyclohexane oxidation over the synthesized catalysts is also disclosed.

2 Experimental

2.1 Preparation of parent MSNs and rod-like SBA-15

The MSNs were synthesized using a surfactant templated, base-catalyzed condensation procedure. Specifically, CTAB (1.02 g, 2.76 mmol) was dissolved in distilled water (480 mL) along with NaOH (3.5 mL, 2 M). The solution was heated to 80 °C before adding tetraethylorthosilicate (TEOS, 5 mL). The reaction mixture was stirred for an additional 2 h at 80 °C. The white precipitate were isolated by filtration and washed with copious amount of water and ethanol. The synthesized MSNs were dried at 100 °C for *ca*. 8 h and then grinded into the powder. Thereafter the surfactant template was kept within the mesochannels of MSNs for the subsequent dissolving of the hydrophobic compounds of Fe (acac)$_3$. Rod-like SBA-15 was prepared by the following procedure: 4.0 g of triblock copolymer Pluronic P123 was added to 150 g of 1.6 M HCl aqueous solution in an autoclave. The mixture was kept under static conditions at 35° C until all the copolymer was completely dissolved. Then 9.2 mL of TEOS was added under vigorous stirring. After about 5 min stirring, the mixture was aged under static conditions for about 20 h. Thereafter the solid products were collected by filtration, washed with water several times and dried at 60 °C for 4 h.

2.2 Preparation of iron doped MSNs (Fe-MSNs) with large pore size

MSNs with expanded pores were prepared using silica/surfactant composite and TMB dissolved with different amount of Fe(acac)$_3$ as swelling agents under hydrothermal conditions. Specifically, dried as-synthesized MSN (1g) was treated with distilled water (30 mL) and the mixture solution was vigorously stirred for about half an hour in an autoclave. Another portion of mixture solution was prepared by dissolving different amount of Fe(acac)$_3$ (40, 60 and 100 mg) in TMB (4 mL). Then the prepared solution was poured into the above autoclave and then heated at 120 °C for 36 h. The resultant MSNs with large pore size and Fe(acac)$_3$ incorporated were collected by filtering the suspension. Then the samples were washed several time with distilled water and ethanol and dried at 100 °C for 24 h. The obtained powder was calcined at 600 °C for 2 h and finally, highly dispersed Fe ions doped MSNs with large pore size were prepared. According to the measured Fe content in MSNs *viz*. 1.01, 1.52, 2.04 wt.- %, the corresponding samples were labeled as Fe-MSNs-1, Fe-MSNs-2 and Fe-MSNs-3 or sample 1, sample 2 and sample 3, respectively.

2.3. Preparation of copper doped SBA-15 (Cu-SBA-15)

The dried rod-like SBA-15 with P123 trapped (about 1g) was treated with 15 mL distilled water and the mixture solution was vigorously stirred for about half an hour in autoclave. Another portion of mixture solution was prepared by dissolving different amounts of Cu(acac)$_2$ in 5mL benzene and 2mL TMB. Then the prepared copper solution was poured into the above autoclave and then heated at different temperatures *viz*. 60, 80 and 100 °C for about 48 h. The resultant Cu(acac)$_2$ infiltrated SBA-15 were collected by filtering the suspension. Then the samples were washed several times with distilled water and ethanol and dried at 100 °C for 24 h. The obtained powder was calcined at 550 °C for 6 h and finally, highly dispersed Cu species doped SBA-15 were prepared. According to the different HT temperatures for Cu(acac)$_2$/SBA-15 mixture solutions and the Cu loading levels calculated from the as-synthesized Cu-SBA-15 catalysts, the corresponding samples were labeled as 60-1, 60-2, 80-1, 80-2, 100-1 and 100-2, respectively (The first numbers of 60, 80 and 100 stand for temperatures, and the second numbers of 1 and 2 respectively represent low and high copper loading levels).

2.4 Characterizations

UV-Visible absorption and diffuse reflectance spectra were recorded on a Shimadzu UV-Vis 3101 spectroscopy. X-ray diffraction (XRD) patterns were collected with Bruker D8 using Cu Kα radiation (40 kV, 40 mA). N$_2$ adsorption-desorption isotherms were obtained on NOVA 4200e at 77 K under a continuous adsorption condition. All samples were pretreated for 12 h at 393 K under nitrogen before measurements. The Brunauer-Emmett-Teller (BET) method was utilized to calculate the specific surface areas using adsorption data in a relative pressure range from 0.2 to 0.4. By using the Barrett-Joyner-Halenda (BJH) model, the pore volumes and pore size distributions were derived from the adsorption branches of isotherms, and the total pore volumes were estimated from the adsorbed amount at a relative pressure P/P_0 of 0.99. The elemental composition was determined by inductively coupled plasma atomic emission spectroscopy (ICP-AES) after the sample was dissolved in a mixture of HF and HNO$_3$. Transmission electron microscopy (TEM) and energy dispersive spectroscopy (EDS) was conducted on a JEM 2100F electron microscope operated at 200 kV. Field emission scanning electron microscopy (FESEM) was performed on JEOL JSM6700F electron microscope. Temperature-programmed desorption of ammonia (NH$_3$-TPD) was performed by using a home-made apparatus. The samples (50 mg) were pretreated at 823 K for 1 h and then cooled down to 100 °C under a He flow. Pure NH$_3$ was injected until adsorption saturation was reached, followed by a flow of He only for 30 min. Then the temperature was raised from 100 °C to 600 °C with a heating rate of 1 degree min^{-1} and the amount of desorbed ammonia was detected by using gas chromatography. Temperature-programmed reduction of hydrogen (H$_2$-TPR) was also performed by using a home-made apparatus loaded with 50 mg of sample. The samples were pretreated at 600 °C for 1 h and then cooled down to 100 °C under a He flow. Pure H$_2$ was injected until adsorption saturation was reached, followed by a flow of He only for 30 min. Then the temperature was raised from 100 °C to 600 °C with a heating rate of 1 degree min^{-1} and the amount of desorbed hydrogen was detected by a TCD.

2.5 Catalytic Evaluation

The alkylation of benzene by BC was used as a model reaction to test the catalytic properties for the synthesized nanocatalysts. The catalytic reactions were performed under N$_2$ in a 50 mL three-necked flask equipped with a reflux condenser and a septum. The temperature of the reaction vessel was maintained using an oil bath. In a typical run, the prepared catalyst (0.1 g) was first activated at 400 °C in air for 4 h and cooled to room temperature prior to their use in the reaction. Then the solid catalyst was introduced into reaction vessel loaded with mixed solution (27.16 mL) of benzene (25 mL) and BC (2.16 mL) (the molar ratio of benzene to BC was kept at 15). The reaction mixture was vigorously stirred and heated to the required temperature (typically 60, 70 and 80 °C). Samples were withdrawn at regular intervals and analyzed using GC-MS (Agilent, 6890/5973N). Since benzene was used in excess, conversion was calculated based on the benzylating reagent, BC. The selectivity is expressed by the molar ratio of formed impurities to converted BC. The catalyst was separated from the reaction solution by centrifugation after the first complete conversion and reused after reactivation at 600 °C for 4 h. The following recycles were performed after each reaction with the same procedures. Generally, the catalytic reactions were repeated for three times to reduce the experimental errors.

The selective oxidation of cyclohexane was carried out in a 100 mL Teflon-lined stainless-steel autoclave. Typically, 8 mL of cyclohexane and 50 mg solid catalyst were added into the reactor. After purging with O_2, the reactor was heated to a predetermined temperature and the O_2 pressure was adjusted to 1MPa with a stirring rate of 100 rpm. During the oxidation process, the O_2 pressure was kept between 0.8-1 MPa. After a predetermined time of reaction, the reactor was cooled down to room temperature and the ethanol was dissolved into the obtained mixture. An excessive amount of triphenylphosphine(Ph_3P) was added to the reaction mixture to completely reduce the cyclohexyl hydroperoxide (CHHP), an intermediate in the cyclohexane oxidation to cyclohexanol. The products were analyzed using a gas chromatography (Perkin-Elmer, Autosystem XL, USA) with a KB-Wax column. The by-products of acids and esters were analyzed by GC-MS (Agilent, 7890A-5975C). Recycling tests in four consecutive reactions were run at 120 °C for 5 h and isobaric condition of 1MPa O_2. After each cyclohexane oxidation run, the solid catalyst was cooled to room temperature and separated by centrifugation from the product solution, and washed with water several times, then dried at 80 °C and reused for the next run under the same conditions. ICP-AES were employed to analyze the copper contents in the filtered liquid product and the used catalysts.

3 Results and Discussion

3.1 Synthetic Strategy

The synthetic protocol used here to incorporate catalytically active centers of iron/copper into the pore channels of MSNs/rod-like SBA-15 is shown in Figure 1. MSNs were firstly prepared by a well reported base catalyzed sol-gel process[22]. After filtering, washing and brief drying, all the impurities were separated and consequently no strong base ions of OH^- were left to attack the later-added iron precursor of $Fe(acac)_3$. MSNs with surfactant retained in the pore channels could maintain their nano-spherical morphology during washing and drying processes and were put into the autoclave for HT with a mixture solution of TMB and $Fe(acac)_3$. Since hydrophobic region of CTAB micelles could serve as an effective carrier for hydrophobic compounds, TMB and $Fe(acac)_3$ were co-infiltrated into the pore channels to expand the pore size and at the same time to introduce the iron species. Iron active centers could be highly and uniformly dispersed within silica framework due to the molecular level dissolution of the precursor compounds into the hydrophobic core of the surfactant template. Similarly Cu ions were introduced in the rod-like SBA-15 using $Cu(acac)_2$ relatively under milder temperature, in order to get highly dispersed Cu ions in side the parent rod-like SBA-15.

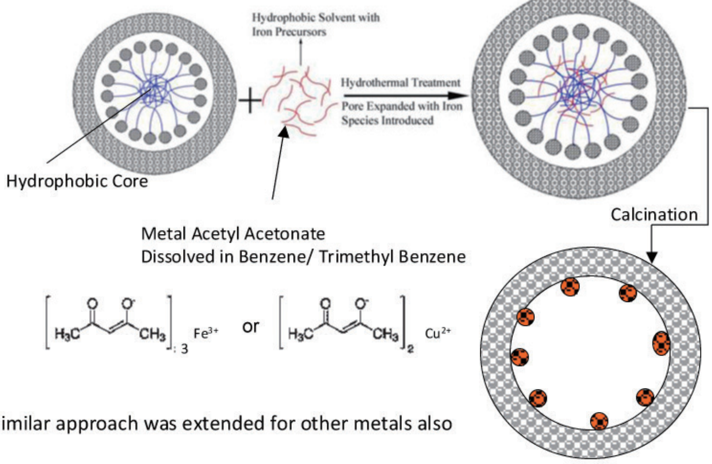

Figure 1 Schematic illustration for incorporating the highly dispersed catalytically active centers into the Mesoporous silica *via* post hydrothermal treatment with TMB and the hydrophobic precursors as a pore expander.

3.2 Structural and Textural characteristics

3.2.1 UV-Vis Spectroscopy

Figure 2 shows UV-Vis spectra that were used to monitor the assembly process for the encapsulation of the hydrophobic compound of metal acetyl acetonate (top) and obtained product after calcination (bottom). Figure 2 (left); The characteristic feature of the spectrum for Fe(acac)$_3$ itself dissolved in ethanol is manifested by the very strong absorption bands at about 240–300 nm due to the transition of a pi–pi* type electrons (b). After HT of MSNs in water solution with TMB and Fe(acac)$_3$ dissolved, it was found that almost the same peaks were present in MSNs suspension using ethanol as a solvent under the same nanoparticle concentrations. Due to the slight difference of micro-environment in the hydrophobic core of surfactant from ethanol solution, the absorption peaks for the encapsulated Fe(acac)$_3$ shift very slightly to the lower wavelength region as shown in the figure. The peak intensity for samples 1, 2 and 3 (Samples 1, 2, 3 or Fe-MSNs-1, Fe-MSNs-2, Fe-MSNs-3) increases gradually, in agreement with the increasing amount of Fe(acac)$_3$ loading. No detectable absorption peak is present in the UV-Vis spectrum for pure MSNs/CTAB composite (a). These results demonstrate that the Fe(acac)$_3$ has been really infiltrated into the hydrophobic core of the surfactant and also verify the synthetic mechanism we proposed.

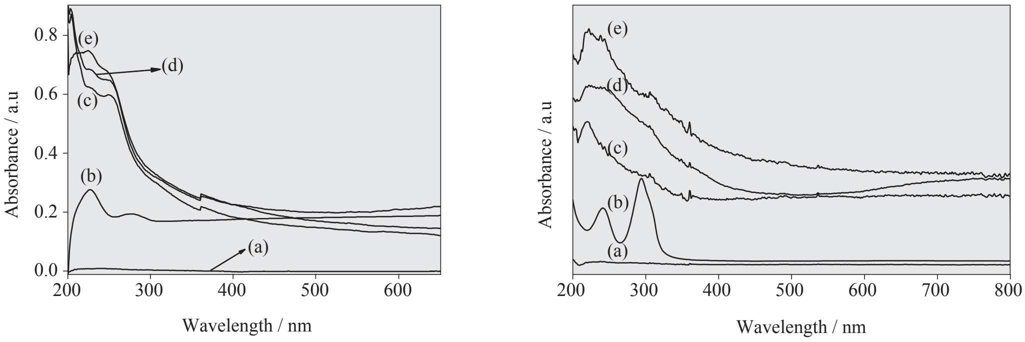

Figure 2 Left; UV-Vis absorption spectra for parent MSNs/CTAB composite (a), fresh Fe(acac)$_3$ dissolved in ethanol solution (b), Fe(acac)$_3$ dissolved in hydrophobic inner core of CTAB surfactant micelles after hydrothermal treatment for Fe-MSNs-1 (c), Fe-MSNs-2 (d) and Fe-MSNs-3 (e).
Right; UV-Vis absorption spectra for the parent SBA-15/P123 (a), pure Cu(acac)$_2$ dissolved in ethanol solution (b), Cu(acac)$_2$ dissolved in hydrophobic inner core of P123 surfactant micelles after hydrothermal treatment for 60-1 (c), 80-2 (d) and 60-2 (e).

Similarly, UV-Vis absorption spectra for the parent SBA-15/P123, pure Cu(acac)$_2$ in ethanol solution, Cu(acac)$_2$ in hydrophobic inner core of P123 surfactant micelles after HT for 60-1, 60-2 and 80-2 samples were exhibited in Figure 2 (right) in order to verify the encapsulation process of the hydrophobic compounds. No obvious absorption peak for the parent SBA-15/P123 is present while all the other samples demonstrate the typical strong absorption bands at about 240–300 nm assigned from Cu(acac)$_2$. Due to the slight difference in micro-environment of the hydrophobic core of surfactant micelles from ethanol solution, the absorption peaks for the encapsulated Cu(acac)$_2$ shift very slightly. These results also manifest that the Cu(acac)$_2$ has been really infiltrated into the hydrophobic core of the surfactant micelles and also verify the synthetic mechanism we proposed. We also found that the peak intensity increased when higher amount of Cu(acac)$_2$ was added into the SBA-15/P123 suspension under the same HT temperature of 60 °C. However, when we increased the temperature to 80 °C (Figure 2 Right (d) or 100 °C (data not shown)), it was found that the loaded Cu(acac)$_2$ in P123 hydrophobic core decreased corresponding to lower peak intensity of the UV-Vis absorption. These observations imply that the treatment at higher temperature is unfavorable for the assembly of the hydrophobic copper compounds into the hydrophobic core of the P123 micelles, assumed that the harsh condition of higher temperature will partially change its inherent hydrophobicity to hydrophilicity, and make the metal organic compounds no longer dissolvable into the hydrophobic cores of surfactant micelle. Since 60 °C was the most optimum temperature of HT based on UV-Vis measurements, our further work was centered on 60-1 and 60-2 samples.

3.2.2 XRD

The small angle XRD was applied to track the ordering evolvement of MSNs and SBA-15 and the effect of pore expansion. As depicted in Figure 3 (left), the well-defined and ordered structure is present for parent MSNs. The sample exhibits hexagonally ordered mesoporous structure that is characteristic of MCM-41-type with (100), (110), and (200) reflections of *p6mm* symmetry. After HT for MSNs in water/TMB mixture with $Fe(acac)_3$ dissolved, all the diffraction peaks for samples 1, 2 and 3 shift to lower angle direction, which indicates the enlarged structure units and pore sizes as we proposed. Three peaks can still be distinguished from all the samples, indicating that the structure ordering was not destroyed during HT. The specific pore structure along with the hexagonal unit cell parameters calculated from XRD for the synthesized samples were listed in Table 1.

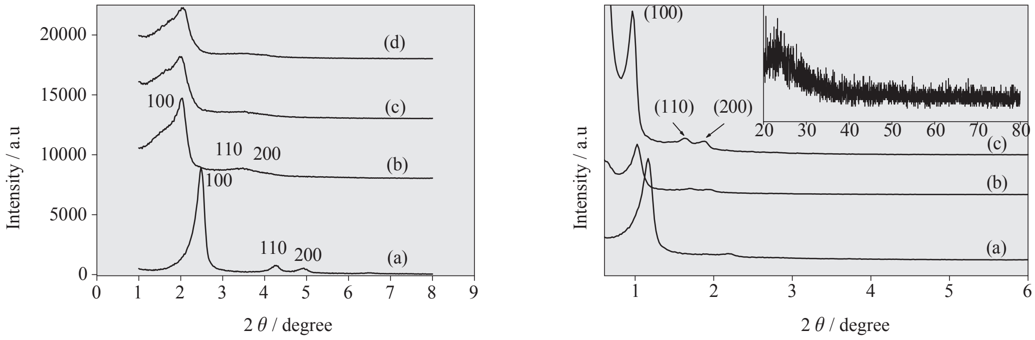

Figure 3 Left; Small angle XRD patterns for parent MSNs (a), Fe-MSNs-1 (b), Fe-MSNs-2 (c) and Fe-MSNs-3 (d). : Right; Small angle XRD patterns of parent SBA-15 (a), 60-1 (b), and 60-2 (c); the inset shows wide angle XRD pattern of sample 60-2.

As manifested in Figure 3 (right), the well-defined and ordered pore structure is present for parent SBA-15. Three well resolved reflections of (100), (110) and (200) could be clearly indexed in the hexagonal space group of *p6mm*. All the diffraction peaks for samples 60-1 and 60-2 shift to lower angle direction, evidencing the enlarged structure units. This provides further evidences that $Cu(acac)_2$ is really effectively incorporated into the hydrophobic region of SBA-15/P123 and expands the pore diameter. Three peaks are perfectly maintained after HT at 60 °C for 48 h, indicating that the structure ordering of the SBA-15 support is not destroyed. In the wide-angle region for 60-2, the sample with the highest Cu content, no diffraction peak corresponding to crystalline CuO clusters could be detected as shown in the inset of Figure 3 (right). It is thus deduced that the particle size of the doped Cu species are probably too small to be detected by X-ray diffraction.

3.2.3 Nitrogen adsorption-desorption measurements

The textural properties of Fe-MSNs with different iron amounts were characterized by nitrogen adsorption measurements. For parent MSNs, the adsorption branch shows a type IV isotherm with sharp capillary condensation steps at a relative pressure of 0.2-0.3 associated with the mesopore filling by N_2 as shown in Figure 4 (top left). The pore size is about 2.4 nm. This is indicative of the presence of mesoporous structure in these materials in consistent with their XRD patterns. After HT, the capillary condensation steps shift to a relative pressure of 0.4-0.55 and pore sizes are obviously expanded to about 3.5 nm for all the iron doped samples as depicted in Figure 4 (top right). Their irreversible type IV adsorption–desorption isotherms with a H1 hysteresis loop indicate their mesoporous channels and narrow pore size distributions. These also indicate that the HT process with swelling agent and $Fe(acac)_3$ did not destroy the structure integrity of the parent MSNs. It is noticeable that the specific surface areas of all the Fe-MSN samples decrease slightly but the pore volume increase significantly, which is also in agreement with the increased pore size of the iron doped samples. The pore structure parameters of the synthesized samples with different copper contents were also characterized by nitrogen sorption isotherms. Consistent with the above XRD analysis, all the samples possess similar N_2 sorption isothermal curves to that of parent SBA-15. Their irreversible type IV adsorption–desorption isotherms with a H1 hysteresis are indicative of the presence of mesoporous structure with narrow pore size distributions. The capillary condensation steps shift to a relatively higher pressure and pore sizes are clearly expanded for all the copper doped samples as depicted in Figure 4 (bottom). This pore size expansion and corresponding pore volume enhancement should be attributed to the introduction of hydrophobic solvent and Cu(acac)$_2$ in hydrophobic core of P123 micelles.

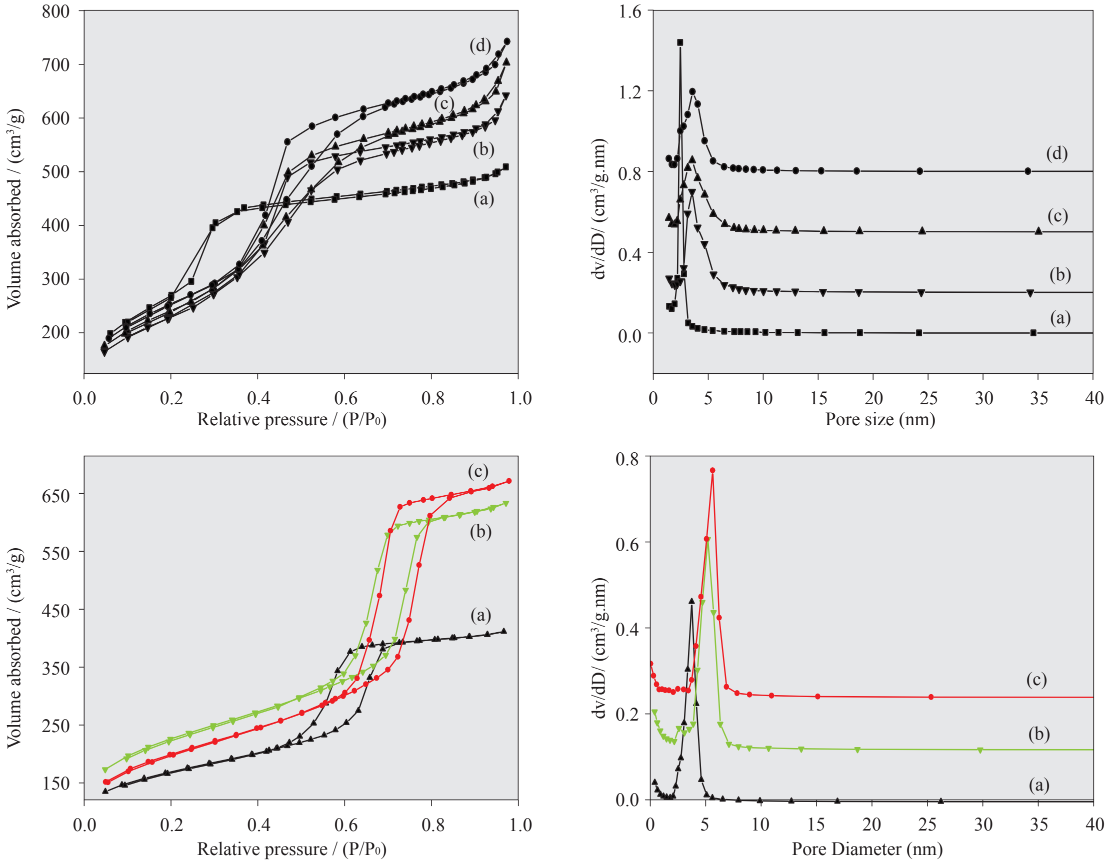

Figure 4 The N_2 adsorption–desorption isotherms (top left) and the corresponding pore size distribution (PSD) (top right) curves for parent MSNs (a), Fe-MSNs-1 (b), Fe-MSNs-2 (c) and Fe-MSNs-3 (d); corresponding isotherm (bottom left) and PSD (bottom right) for the samples of parent SBA-15 (a), 60-1 (b) and 60-2 (c).

Table 1 Pore structure parameters and the Fe contents in MSNs.

Samples	S_{BET} / m^2/g	D_{BJH} / nm	Pore volume / cm^3/g	d^a_{100} / nm	a_0^b / nm	Theoretical Fe / wt%^{c}	ICP Fe / wt%
MSNs	1012	2.4	0.84	3.44	3.97	0	0
Fe-MSNs-1	912	3.5	1.19	4.21	4.86	1.12	1.01
Fe-MSNs-2	881	3.5	1.12	4.29	4.95	1.76	1.52
Fe-MSNs-3	847	3.5	1.03	4.18	4.82	2.83	2.04

d^a_{100} was calculated from the XRD; $a_0^b = 2d/3^{1/2}$ was the hexagonal unit cell parameter; ^{c} Theoretical iron content was calculated from the initial composition for Fe-MSNs synthesis.

Table 2 Pore structure parameters and the Cu content in rod-like SBA-15.

Sample	S / m^2/g	Pore width / nm	Pore volume / cm^3/g	Cu / wt.%
SBA-15	614	4.6	0.65	0
60-1	687	5.9	1.00	0.19
60-2	690	6.4	1.05	0.85

The specific pore structure parameters as well as precise amounts of iron and copper loading level in different samples measured by ICP-AES are included in Table 1 and Table 2, respectively.

3.2.4 SEM/TEM

For Fe-MSNs-1, SEM image shows that the isolated MSNs with a mean diameter of *ca*. 100 nm were obtained as shown in Figure 5a. The particles are relatively uniform and size distribution is relatively narrow. To the best of our knowledge, this is the first report of the MSNs with the pore diameter as large as 3.5 nm with iron active centers simultaneously incorporated in the silica framework. From TEM image of sample 1, it is clearly observed that MSNs are mainly spherically shaped and mesopores with diameter of about 3.5 nm are clearly seen in the enlarged images. For Fe-MSNs-2, discrete spherical particles with a size of around 80–110 nm can be also observed from SEM image. Interestingly, the parallel pore channels also cross through the whole area of nanoparticles like sample 1 as shown in Figure 5e. We could find some very short rod-like nanoparticles with oblate shape for Fe-MSNs-3 (Figure 5g). The 1D hexagonal mesoporous ordering could be clearly identified from the magnified image of Figure 5h. The pore channels are parallel to each other and along the axis direction of the short nanorods. These studies give further support that the long period ordering of the mesostructure has been largely retained in the synthesized samples after iron doping.

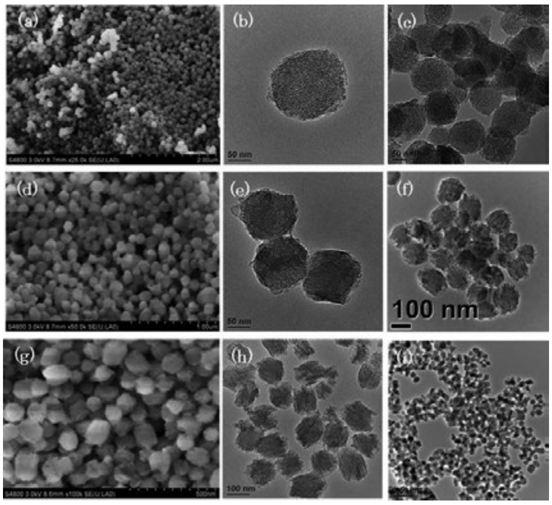

Figure 5 Typical SEM and TEM images for the synthesized iron doped MSNs; a, d and g are SEM images for samples 1, 2 and 3, respectively; c, f and i are TEM images for samples 1, 2 and 3 respectively, and b, e and h are corresponding enlarged images.

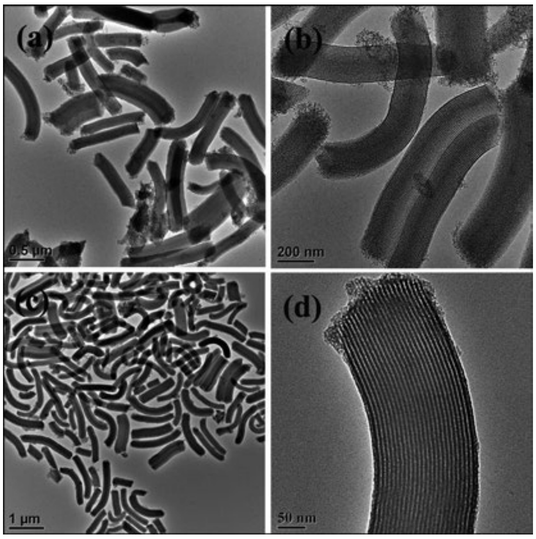

Figure 6 Typical TEM images for the parent SBA-15 (a), 60-1 (b) and 60-2 (c) samples; the enlarged image of Cu-SBA-15 rods in sample 60-2 (d).

Figure 6 exhibits the TEM images of the parent SBA-15 and copper doped samples, viz. 60-1 and 60-2. SBA-15 rods with meso-channels are clearly present for all the samples including parent and Cu doped SBA-15, which indicates that the introduction of copper oxide did not destroy the ordered mesostructure and the discrete rod-like morphology of the parent SBA-15. The preservation of the mesostructure ordering could be more clearly visible from the enlarged image of Figure 6d and parallel channels cross through the whole SBA-15 rods.

It is evidenced from Figures 5 and 6 that no Fe_2O_3 or CuO particles can be found outside or inside the channels, even for sample with the highest metal content, which means that no aggregation or visible particles formed. Therefore, it is concluded that uniform and highly dispersed metal species were successfully introduced into the framework of silica, which benefited from the molecular level dissolution of metal acetylacetonate into the hydrophobic cores of surfactant micelles. This also verifies that introduced metal active centers are highly accessible to guest molecules as the mesochannels are unblocked by introduced metal species evidenced by the TEM images.

3.2.5 Acidity (NH_3-TPD) and Reducibility (H_2-TPR)

The relative amount of the acid sites of the synthesized Fe-MSNs were studied by NH_3-TPD since it is a useful technique to roughly evaluate the acid strength by measuring the temperatures at which TPD peaks are observed. All the NH_3-TPD profiles for iron doped MSNs are shown in Figure 7 (top), and the profile for pure MSNs is also shown in Figure 7d for comparison. It can be found that there exist two broad desorption curves, the first one appears around 150 ℃ attributed to the weakly adsorbed ammonia and the second broad desorption peak (Temperature range of 200 – 550 ℃ with a $T_{max} \sim 320$ ℃) is due to acidity of the samples, along with tail-like desorption at around 550 ℃. Actually, since ammonia is such a strong base (pK_b is about 5) that it reacts even with extremely weak acid sites, therefore, we found that even for pure silica (Figure 7d), a small NH_3 desorption peak was also present. However, the acidic site quantities of iron doped MSNs, corresponding to the total acidity, are much higher than that of pure MSNs. It is clearly revealed from the patterns presented in the Figures that the desorption peak intensity in the temperature range of 200-550 ℃ increases with the increasing iron content. The larger amount of acidity of Fe-MSNs-3 is believed to be resulted from the presence of relatively high amount of well dispersed Fe^{3+} ions in the silica framework.

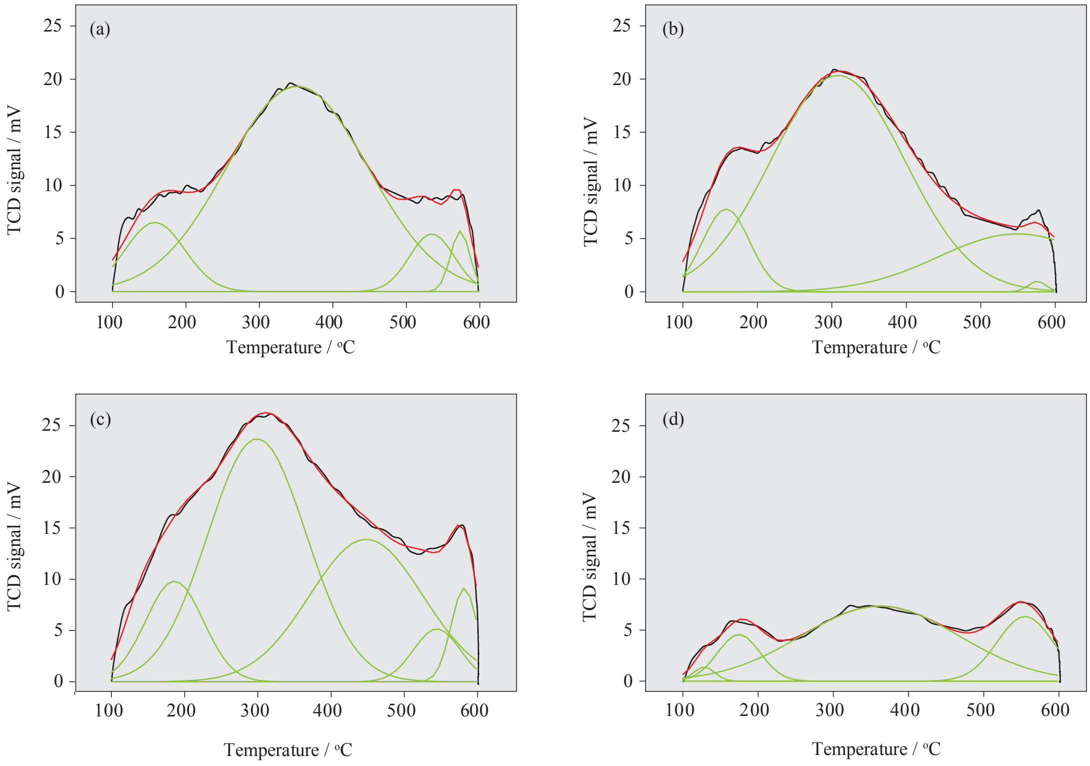

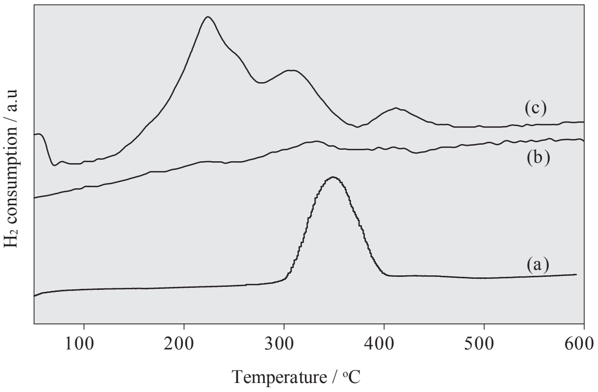

Figure 7 Top; NH$_3$-TPD curves of parent and iron doped MSNs for sample 1 (a), sample 2 (b), sample 3 (c) and parent MSNs (d). The scale for y axis was set to be uniform for comparison. The red line is gauss fit for the original data and the green lines are deconvolution curves for NH$_3$-TPD profile. Bottom; H$_2$-TPR profiles for the bulk CuO (a), 60-1 (b) and 60-2 (c) samples.

TPR measurements were carried out to investigate the reducibility of the copper species. Figure 7 (bottom) presents the hydrogen reduction profiles of samples 60-1, 60-2 as well as bulk CuO. Three hydrogen consumption peaks exhibit for sample 60-2 catalyst. The peak at 225 °C could be assigned to highly dispersed copper species such as oxocations (Cu-O-Cu)$^{2+}$ while the reduction peak at 306 °C could be ascribed to the small CuO clusters at the inner surface of SBA-15. It should be emphasized that the cylindrical mesopores of SBA-15 are generally surrounded by a corona, which may represent either a microporous layer or some surface corrugations of the pore wall. The introduction of the copper species might smooth the corrugated inner surface of the synthesized SBA-15. A very weak signal at 411 °C with small peak area (The ratio to the total peak area is less than 5 %), which is shifted to higher temperature as compared to bulk CuO with a reduction temperature of 360 °C (Figure 7a; bottom), is most probably attributed to the isolated CuO in the SBA-15 framework. Very weak hydrogen consumption signals for sample 60-1 is corroborating to the very low copper content in the sample but is still distinguishable at almost the same positions as sample 60-2.

3.3 Catalytic Properties

The catalytic activity and selectivity of the Fe-MSNs were tested for the liquid phase benzylation of benzene by BC, which holds the key importance for the production of diphenylmethane (DPM) or related compounds in pharmaceutical intermediates or fine chemical industry. Conversion is calculated based on BC and Figure 8 shows the conversion of BC as a function of reaction time over Fe-MSN samples under a mild reaction temperature of 60 °C. It could be found that the reaction time needed for 100 % conversion of BC was not longer than 60 min for all the three samples, and it decreases from 60 to 30 min with the increasing Fe loading amount, which is remarkably shorter than those reported[23]. As a control experiment, we did not detect any DPM converted from benzylation of benzene by BC over pure MSNs. These demonstrate that the Fe-MSNs are highly efficient for the current investigated catalytic reaction, and the catalytic activity is evidently increased with iron content. Although the coordination environment of Fe ions in sample 1, 2 and 3 are slightly different from each other, they all exist in a less coordinatively saturated status, which are highly active for the benzylation of benzene. This is believed to be benefited from the intrinsic advantages of our synthetic strategy in which the molecular level dissolution and uniform distribution of the precursor compounds in the hydrophobic core of the surfactant template were achieved.

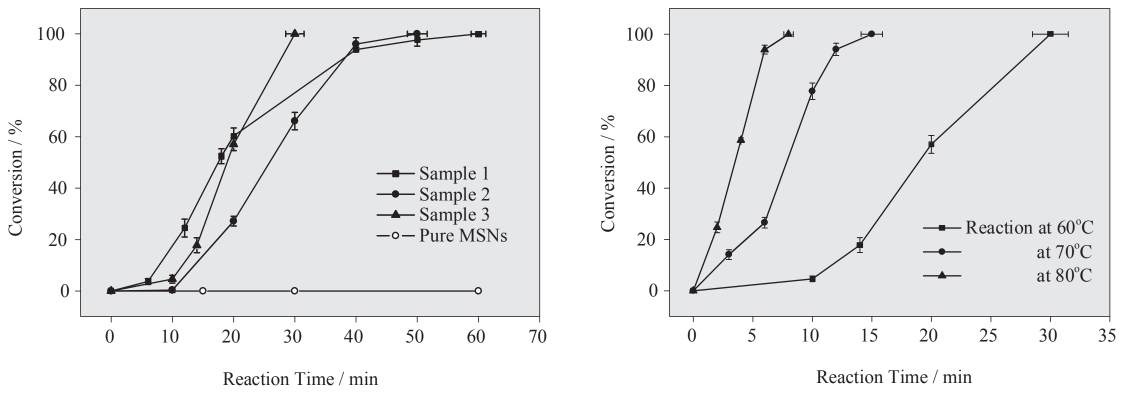

Figure 8 Left;Conversion of BC *vs*. reaction time on various samples with different iron loading amount at 60 °C. Right;Effect of reaction temperature on the conversion of BC in the benzylation of benzene over Fe-MSNs-3 nanocatalyst.

It has been reported[23] that a long reaction time of 400 min. was needed to obtain complete conversion of BC and 98.9 % selectivity to DPM was achieved by using Fe-HMS as catalyst with almost the same Fe content as in our synthesized Fe-MSNs-3. Compared to those reported catalysts, our samples present higher yield of DPM and much shorter reaction time. We do believe that such a higher activity and selectivity can be attributed not only to the highly dispersed iron catalytically active centers, but also to the nanometric particle size and the enlarged pore channels of the synthesized catalysts, leading to the full accessibility of the active irons to reactant molecules. To further evaluate the catalytic performance of sample 3, its catalytic reactivity was tested at higher temperatures to detect whether the catalytic efficiency could be further enhanced. Figure 8 right shows the effect of the reaction temperature on catalytic activity. It can be obviously found that an increase in reaction temperature gives rise to a remarkable enhancement of catalytic activity. When the temperature was set to 80 °C, the reaction was rapidly completed in a very short time period of ca. 8 min, in sharp contrast to the 30 min duration when reacted at 60 °C. The selectivity to DPM was also high, and up to 95 % conversion was achieved at a reaction temperature of 80 °C.

The stability of Fe-MSNs-3 was also evaluated and the yields of the fresh and reused nanocatalyst in the benzylation of benzene by BC reacted at 70°C were presented in Table 3. It was found that even after three time runs, there was no significant loss in its catalytic properties, either activity or selectivity. Such catalytic characteristic is of great importance for potential industrial application. It is important to remark that the nanocatalyst has to be regenerated by re-calcination to get rid of the organic species adsorbed on the catalyst surface and to maintain the activity for the successive runs.

Table 3 Catalytic performance of the fresh and recycled Fe-MSNs-3 nanocatalyst in the benzylation of benzene at 343 K.

Catalyst	Time / min	Conversion / %	Selectivity / %
fresh	15	100	98.7
First reuse	15	98	95.4
Second reuse	15	94	93.7

Copper could serve as the active center for many heterogeneous redox reactions, currently there are only few studies to utilize synthetic copper catalysts for the selective oxidation of cyclohexane oxidation. Herein we tested the catalytic properties of the Cu-SBA-15 for the selective oxidation of cyclohexane. The reaction is of increasing importance because it is one of methods to produce cyclohexanone (K) and cyclohexanol (A) (ketone/alcohol or K/A oil), which are starting materials in the manufacture of nylon-6 and nylon 6,6 polymers. The traditional commercial process for cyclohexane oxidation using molecular oxygen or air is generally carried out under relatively harsh condition at a temperature of 150-160 °C and an oxygen pressure of 1-2MPa, affording about 4 % conversion and 70-85 % selectivity to cyclohexanone and cyclohexanol. The specific reaction process is shown in Scheme 1.

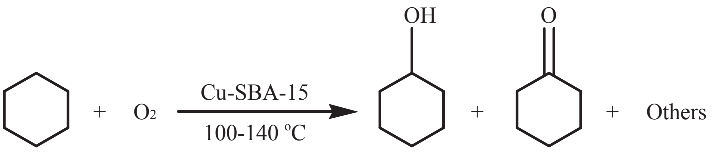

Scheme 1 Chemical equation for the cyclohexane oxidation over the synthesized Cu-SBA-15 catalysts.

Firstly, we compared the catalytic performances for cyclohexane oxidation under a temperature of 120 °C and oxygen pressure of 1MPa over the synthesized Cu-SBA-15 with different copper content and the results were listed in Table 4. A low conversion of 3.6 mol.% was obtained over 60-1 catalyst. For 60-2 catalyst with 0.85 wt.% Cu, the conversion of cyclohexane reached to 9.5 mol.%. As a control experiment, we did not detect any K/A oil converted from cyclohexane oxidation without using the copper catalysts. These suggest that the contents of Cu in the synthesized catalysts have a crucial influence on their activity in cyclohexane oxidation.

Table 4 Properties of the different catalysts for the cyclohexane oxidation reaction.

Catalysts	Cyclohexane conversion / mol.%	Products selectivity / mol.%		
		Cyclohexanol / A	Cyclohexanone / K	By-products
blank	—	—	—	—
60-1	3.6	48.7	47.9	3.4
60-2	9.5	31.8	49.4	18.8

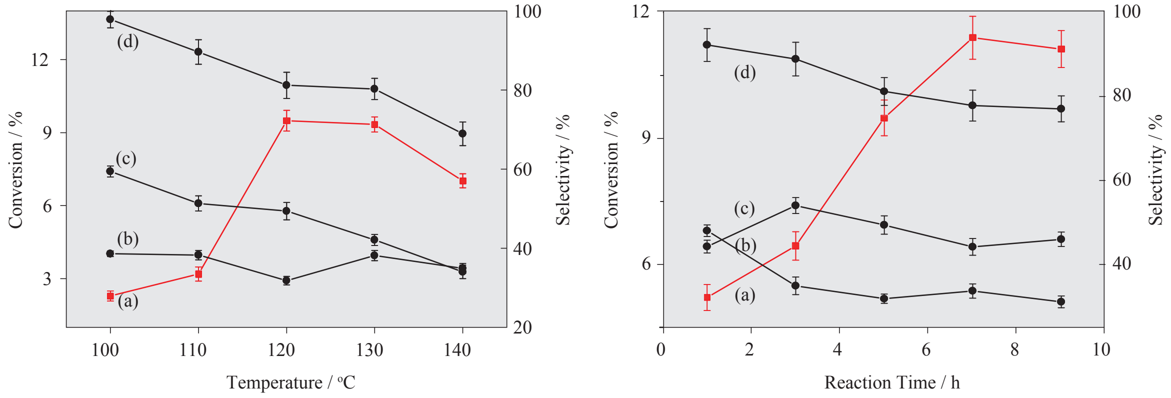

Reaction conditions: cyclohexane 8mL, catalyst 50mg, oxygen 1MPa, temperature 120 °C, reaction time 5h. By-products mainly include adipic acid, valeric acid, formic acid cyclohexyl ester and pentanoic acid cyclohexyl esters.

Figure 9. Left; Effect of reaction temperature on conversion and selectivity in cyclohexane oxidation over 60-2 catalyst for the conversion of cyclohexane (a); selectivity of cyclohexanol (b); selectivity of cyclohexanone (c); selectivity of cyclohexanol and cyclohexanone (d). Reaction conditions: cyclohexane 8 mL, catalyst 50 mg, oxygen pressure 1MPa, reaction time 5h. Right;. Effect of reaction time on conversion and selectivity in cyclohexane oxidation over sample 60-2 for conversion of cyclohexane (a); selectivity to cyclohexanol (b); selectivity to cyclohexanone (c); selectivity to cyclohexanol and cyclohexanone (d). Reaction conditions: cyclohexane 8 mL, Cu-SBA-15 catalyst 50 mg, oxygen pressure 1 MPa, temperature 120 °C

Figure 9 presents the effect of the reaction temperature on the cyclohexane oxidation over 60-2 catalyst with time duration of 5h and isobaric condition of 1MPa oxygen. It can be found that the conversion of cyclohexane increases quickly while increasing the reaction temperature from 100 to 120 °C and reaches a maximum of 9.5 mol.% at 120 °C. Subsequently, the conversion gradually drops to a lower value of 7.0 mol.% at 140 °C, which is most probably due to the decrease of oxygen amount at increased temperature under isobaric conditions. Meanwhile, at initial stage, the selectivity of K/A oil goes down with the increase of temperature. The distribution of cyclohexanone also gets to its maximum of 59.4 % at 100 °C and the change trend is similar with that of selectivity to K/A oil. However, as reaction temperature increases, the distribution of cyclohexanol remains nearly unchanged while the molar ratio of K to A goes down when the temperature is increased, which suggests that cyclohexanone is continuously oxidized to by-products. Generally, the acid and ester are the products of deep oxidation of K/A oil. The distributions of these by-products increase with increasing temperature, indicating that, at higher temperature, oxidation rate of the cyclohexane to the desired products is slower than that of K/A oil oxidation to by-products. Thus, temperature higher than 120 °C has a negative effect on both conversion and selectivity. To maintain a high yield to the desired products, a relatively mild reaction temperature of 120 °C seems most suitable for the current synthesized Cu-SBA-15 catalysts.

To further probe the optimum reaction condition for the synthesized 60-2 sample, the effect of reaction time on cyclohexane conversion and product distributions at reaction temperature of 120 °C and oxygen pressure of 1 MPa was explored and shown in Figure 9 right. It can be found that the cyclohexane conversion steadily increased with increasing reaction time and reached as high as 11.4 mol.% in 7 h, while prolonging the reaction time beyond 7 h, the increasing trend got flattened. In addition, the selectivity of K/A oil rose to its maximum of 92.3 % in 1 h, and decreased gradually with further increasing reaction time, which was most possibly due to the further oxidation of cyclohexanol and cyclohexanone by molecular oxygen. Obviously, a long reaction time was unfavorable for the selective production of K/A oil.

Table 5 Effect of recycling of sample 60-2 on the catalytic properties in the cyclohexane oxidation reaction.

Cycle of Catalysts	Cyclohexane conversion / mol.%	Products selectivity / mol.%		
		Cyclohexanol / A	Cyclohexanone / K	By-products
First (fresh)	9.5	31.8	49.4	18.8
Second	8.8	30.8	46.7	22.5
Third	8.5	29.9	46.0	24.1
Fourth	4.4	43.0	33.1	23.9

The cycling is one of the important aspects for practical applications. The reusability of Cu-SBA-15 catalyst in the oxidation of cyclohexane has been examined under the optimum conditions of 120 °C and 1MPa O_2. The results in Table 5 show that the conversion did not change so much with a value around 9% and the selectivity slightly decreased from 81.2% to 76.0% even after three runs. ICP-AES analyses of the filtered liquid product and the used catalysts did not detect the obvious leaching of the copper ions from the synthesized 60-2 sample. These further confirm the stability and recyclability of the synthesized catalysts for the oxidation of the cyclohexane with oxygen in a solvent-free system.

4 Conclusions

We have developed an effective post HT strategy to dope the highly dispersed iron active centers into the framework of MSNs, and in the meantime, the pore diameter of the synthesized MSNs was successfully expanded to *ca*. 3.5 nm, which facilitated the diffusion of the guest molecules and benefited to the catalytic reactions involving bulky reagents. As the swelling agents worked during post HT for the formed nanospheres, the nanoscale morphology was perfectly retained. The medium and strong acidic site quantities of Fe-MSNs were quite high and their values increased with the iron content increasing. Benefiting from the high amount of acidic sites, enlarged pore diameter and nanometric pore channel length, the synthesized nanocatalysts demonstrated high catalytic activity and selectivity for the liquid phase benzylation of benzene by benzyl chloride. Using this strategy, highly dispersed copper species into the pore channels of mesoporous SBA-15 were doped and the key to the success in synthesizing the catalysts is to encapsulate the hydrophobic Cu(acac)$_2$ into purified SBA-15/P123 during post hydrothermal treatment, in which copper precursor is unaffected by the harsh reaction environment such as strong acid media employed for SBA-15 synthesis. The synthesized catalysts demonstrated enhanced catalytic activity for cyclohexane oxidation. It is clear that this newly developed route is general to introduce different highly dispersed metallic active centers by choosing the proper metallic precursor compounds dissolvable in TMB, and simultaneously, to expand the pore diameter.

References

1) C. T. Kresge, M. E. Leonowicz, W. J. Roth, J. C. Vartuli, J. S. Beck, *Nature,* **359**, 710 (1992).

2) J. S. Beck, J. C. Vartuli, W. J. Roth, M. E. Leonowicz, C. T. Kresge, K. T. Schmitt, C. T. W. Chu, D. H. Olson, E. W. Sheppard, S. B. McCullen, J. B. Higgins, J. L. Schlenker, *J. Am. Chem. Soc.,* **114**, 10834 (1992).

3) J. L. Gu, Y. Huang, S. P. Elangovan, Y. S. Li, W. R. Zhao, T. Iijima, Y. Yamazaki, J. L. Shi, *J.Phys.Chem.,* C **125**, 21211 (2011).

4) J. L. Gu, X. Dong, S. P. Elangovan, Y. S. Li, W. R. Zhao, T. Iijima, Y. Yamazaki, J. L. Shi, *J.Solid State Chem.,* **186**, 208 (2012)

5) D. J. Mihalcik, W. B. Lin, *Angew. Chem. Int. Ed.,* **47**, 6229 (2008).

6) M. Kruk, M. Jaroniec, A. Sayari, *J. Phys. Chem. B,* **103**, 4590 (1999).

7) A. Sayari, Y. Yang, M. Kruk, M. Jaroniec, *J. Phys. Chem. B,* **103**, 3651 (1999).

8) A. Ahmed, R. Clowes, E. Willneff, H. Ritchie, P. Myers, H. Zhang, *Ind. Eng. Chem. Res.,* **49**, 602 (2010).

9) J. L. Gu, J. L. Shi, L. M. Xiong, H. R. Chen, L. Li, M. L. Ruan, *Solid State Sci.,* **6**, 747 (2004).

10) P. N. Minoofar, R. Hernandez, S. Chia, B. Dunn, J. I. Zink, A. C. Franville, *J. Am. Chem. Soc.,* **124**, 14388 (2002).

11) R. H. Holm, F. A. Cotton, *J. Am. Chem. Soc.,* **80**, 5658 (1958).

12) C. M. Chanquía, L.,Andrini; J. D. Fernandez, M. E. Crivello, F. G. Requejo, E. R. Herrero; G. A Eimer. *J. Phys. Chem.* C, **114**, 12221 (2010).

13) A. Taguchi; F. Schuth, *Microporous Mesoporous Mater.,* **77**, 1 (2005).

14) I. J.Drake, K. L. Fujdala, S. Baxamusa; A. T. Bell; T. D. Tilley, *J. Phys. Chem. B,* **108**, 18421 (2004).

15) C. K.Chen, Y. W. Chen; C. H. Lin, H. P. Lin; C. F. Lee, *Chem. Commun.,* **46**, 282 (2010).

16) Patel, A.; Rufford, T. E.; Rudolph, V.; Zhu, Z. H. *Catal. Today,* **166**, 188 (2011).

17) C. M. Chanquía, K. Sapag; E. R. Castellon; E. R. Herrero; G. A. Eimer, *J. Phys. Chem. C,* **114**, 1481 (2010).

18) P. N. Minoofar, R. Hernandez; S. Chia; B. Dunn, J. I. Zink; A. C. Franville, *J. Am. Chem. Soc.,* **124**, 14388 (2002).

19) D. Y. Zhao, J. L. Feng; Q. S. Huo; N. Melosh, G. H. Fredrickson; B. F. Chmelka, G. D.Stucky, *Science,* **279**, 548 (1998).

20) L.Liu, Y. Li, H. Wei,; M. Dong; J. Wang, A. M. Z. Slawin, J. Li, J. Dong; R. E. Morris, *Angew. Chem. Int. Ed.,* **48**, 2206 (2009).

21) Y. Sun, S. Walspurger, J. P. Tessonnier, B. Louis, J. Sommer, *Appl. Catal. A,* **300**, 1 (2006).

22) C. Y. Lai, B. G. Trewyn, D. M. Jeftinija, K. Jeftinija, S. Xu, S. Jeftinija, V. S. Y. Lin, *J. Am. Chem. Soc.,* **125**, 4451 (2003).

23) K. Bachari, J. M. M. Millet, B. Benaichouba, O. Cherifi, F. Figueras, *J. Catal.,* **221**, 55 (2004).

Dr. S. P. Elangovan
Chemical Products R&D Department

Dr. Jinlou Gu
Associate professor
East China University of Science and Technoligy